IOP Publishing Journal of Physics B: Atomic, Molecular and Optical Physics
J. Phys. B: At. Mol. Opt. Phys. **53** (2020) 045202 (8pp) https://doi.org/10.1088/1361-6455/ab5904

# Probing photon interaction with $H_2O$ and $D_2O$

**Paresh Modak and Bobby Antony**

Atomic and Molecular Physics Lab, Department of Physics, Indian Institute of Technology (Indian School of Mines), Dhanbad-826004, Jharkhand, India

E-mail: bobby@iitism.ac.in

Received 13 September 2019, revised 30 October 2019
Accepted for publication 19 November 2019
Published 24 January 2020

**Abstract**

Investigation of the valence state photoionization of water using vacuum ultraviolet and soft x-rays gives important information for spectroscopic analysis and studies of radiation loss and cell biology. In this article, the total and valence-shell photoionization cross sections of $H_2O$ and $D_2O$, generating the states $^2B_1$, $^2A_1$ and $^2B_2$, and their isotopic consequences are studied. The effect of bonding on valence state photoionization is also reported. The calculations were made using R-matrix theory for photon energies up to 40 eV. Electronic transitions below 20 eV were considered to account for the autoionizing Rydberg transitions. This is the first report to demonstrate the effect of bonding on valence state photoionization. For the isotopic partner ($D_2O$), we observed a quantitative change in cross section. Comparisons are made with the previously available results and a reasonable agreement is found. The present study gives a comprehensive understanding of the photoionization of water, thus providing deep insight into different non-dissociative processes of the molecule in various environments.

Keywords: photoionization, $H_2O$, R-matrix method, autoionization

(Some figures may appear in colour only in the online journal)

## 1. Introduction

When photons interact with a molecule, various processes such as excitation, ionization and fragmentation occur depending on the energy of the primary photon. Such interaction provides a rich spectrum of data. Analysis of these spectroscopic data gives remarkable information about these processes, which in turn helps us understand the photochemistry of the environment. Moreover, due to the complex features in the photoionization spectrum, data from molecular photoionization processes has many applications in various fields of applied sciences including aeronomy, planetary science, radiation chemistry and physics and biology [1], particularly for theoretical modeling. Photoionization is the primary source of ions produced in the interstellar medium and the upper atmosphere of astral bodies. The chemical and physical properties of the isotopic counterpart of a molecule often deviate from those of its normal partner. Thus, we observe a change in the intensities of absorption spectra, reaction rates and atmospheric escape velocities. Therefore, photoionization data for a molecular species and its isotope are a key parameter in the modeling of various environments such as planetary atmospheres, interstellar molecular clouds and solar nebulas [2]. Such data can also be utilized to interpret the chemical and physical properties and reaction pathways in these environments. Therefore, total and partial cross section data are a primary requirement for the evaluation of experimental data on molecular photoionization. Besides, photoionization data are enriched with sharp features near the threshold, which represent autoionizing Rydberg transitions. These states cannot be produced experimentally due to the practical difficulty of producing a narrow-bandwidth (natural line width) photon beam. Hence, the experimental results greatly play down the presence of such transitions. This problem can be fixed with a theoretical study. Theoretical calculation of total and partial photoionization cross sections has been improving steadily due to the development of precise computational methods and the availability of high-speed computers.

The photo-processes of water have fascinated researchers for decades due to the abundance of water in many environments and its role as a greenhouse gas. Photon-induced

 

cross sections of water vapor in a vacuum are important in the study of the physics and astronomy of the upper atmosphere [3]. Knowledge about the photoionization of water is also important in the study of radiation damage in biological cells [4]. Heavy water is widely used as a coolant in nuclear reactors, and hydrated electrons have fascinated scientists for a long time [4].

We have studied photoionization of water ($H_2O$) and its isotopic counterpart ($D_2O$) from three outer valence orbitals $1b_1$, $3a_1$ and $1b_2$. Of particular interest for the present study is the $1b_2$ orbital and the effect of bonding on valence state photoionization. The present photoionization cross section can be represented considering three outer valence orbitals of the target molecule as

$$X_2O + h\nu \rightarrow X_2O^+(^2B_1, 1b_1^{-1}) + e^-$$
$$X_2O + h\nu \rightarrow X_2O^+(^2A_1, 3a_1^{-1}) + e^-$$
$$X_2O + h\nu \rightarrow X_2O^+(^2B_2, 1b_2^{-1}) + e^-$$

where X is H or D.

A number of theoretical calculations and experimental observations of the photon-induced cross section of $H_2O$ and $D_2O$ have so far been performed. There are experimental results from Katayama *et al* [3] who used a photoelectric scanning technique, Dutuit *et al* [5] who used direct photoionization, Hadad *et al* [6] who used a double ionization chamber, Truesdale *et al* [7] who employed time-of-flight photoelectron spectroscopy and Tan *et al* [8] who used electron-impact coincidence simulation techniques. Theoretical results have been reported by Cacelli *et al* [9] using random phase approximation, Stener *et al* [10] employing a time-dependent density-functional theory (TD-DFT) approximation and Novikovskiy *et al* [11] who used the single-center (SC) method based on numerical integration of the coupled Hartree–Fock equations. A review of the literature suggests that these are the most important and recent sets of data to be considered for comparison with the present R-matrix results.

## 2. Theory

The present calculations were performed using the UK polyatomic R-matrix method [12]. The basic idea of the R-matrix method is to divide the configuration space into two regions: an inner region where exchange-correlation is important and an outer region where no exchange takes place but only multipole potential of the target is important. The two regions are separated by a spherical boundary in configuration space. Using this approach the collision problem in the inner region can be solved like a bound state problem and the solution for the outer region is obtained for each continuum electron energy using a set of close-coupled equations. The R-matrix connects these two regions at the boundary. The inner region is defined by a sphere, centered at the center of mass of the target molecule. The effect of polarization is adjusted considering pseudo-states over valence orbitals. At intermediate energies this is a reliable procedure to address the issue of electron–electron correlation in *ab initio* calculations. The electronic states of target molecular ion are represented using a multiconfigurational state function as in the case of electron–molecule collisions. These functions very well describe the bound states as well as the correlation between initial and final states.

For the present calculation we used time-reversal symmetry of photoionization, which enables us to study the photoionization process in terms of electron–ion collisions. The differential cross section for photon ionization of a molecule in the length gauge dipole approximation is represented as [13]

$$\frac{d\sigma_{if}}{d\boldsymbol{k}_f} = 4\pi^2\alpha a_0^2\omega|\boldsymbol{d}_{if}(\boldsymbol{k}_f).\hat{\epsilon}|^2 \tag{1}$$

where $\alpha$ is the fine structure constant, $a_0$ is the Bohr radius, $\omega$ is the photon energy in atomic units and $\hat{\epsilon}$ is the direction of polarization of the incident photon in the molecular frame. $\boldsymbol{d}_{if}(\boldsymbol{k}_f)$ is the transition dipole between the initial state $i$ and a single continuum state $f$ in the molecular frame and this can be expressed as a function of the ejected electron momentum, $\boldsymbol{k}_f$;

$$\boldsymbol{d}_{if}(\boldsymbol{k}_f) = \langle\psi^{(-)}_{fk_f}|\boldsymbol{d}|\phi^N_i\rangle \tag{2}$$

where $\psi^{(-)}_{fk_f}$ is the final continuum state, $\phi^N_i$ is the initial bound state and $\boldsymbol{d}$ is the dipole operator, which, again can be represented in spherical vector form using length gauge as:

$$\boldsymbol{d}_q = (4\pi/3)^{1/2}\sum_{i=1}^{N} r_i Y_{1,q}(\hat{r}_i). \tag{3}$$

Here $q = \pm 1$ for circularly polarized photons and $q = 0$ for linear polarization. For bound states of a neutral target, equation (2) is confined to the inner region and both the initial and final states are expanded as

$$\Phi^{(N)}_i = \sum_k B_{ik}\psi^{(N)}_k \tag{4}$$

$$\psi^{(-)}_{fk_f} = \sum_k A_{fk}(\boldsymbol{k}_f)\psi^{(N)}_k. \tag{5}$$

These are the energy-dependent solutions for initial and final states, respectively. Now, equation (3) can be written in terms of the solution of an initial and final state as

$$\boldsymbol{d}_{if}(\boldsymbol{k}_f) = \sum_{kk'} A^*_{fk}(\boldsymbol{k}_f)\langle\psi^{(N)}_k|\boldsymbol{d}|\psi^{(N)}_{k'}\rangle B_{ik'}. \tag{6}$$

In the R-matrix formulation, this is defined in the angular momentum basis for the ejected electron. Expanding equation (6) in terms of partial waves gives:

$$\boldsymbol{d}_{if}(\boldsymbol{k}_f) = \sum_{kk'}\sum_{l_f m_f} i^{-l_f}e^{i\sigma_{l_f}}Y_{l_f,m_f}(\hat{\boldsymbol{k}}_f)$$
$$*A^*_{fl_f m_f,k}(E)\langle\psi^{(N)}_k|\boldsymbol{d}|\psi^{(N)}_{k'}\rangle B_{ik'} \tag{7}$$

where $\sigma_{l_f}$ is the Coulomb phase, $\arg(\Gamma(l_f + i\eta_f + 1))$, where $\eta_f = -\frac{Z-N+1}{k_f}$, and $Z - N + 1$ is the residual charge of the system. The Clebsch–Gordon coefficient deals with the spin coupling of the continuum electron and the ion. Transforming all equations into the laboratory frame using Wigner rotation

**Table 1.** SCF total and orbital energies of $X_2O$ (in au).

| Orbital | Present $H_2O$ | Present $D_2O$ | Basis set 115[a] [17] | GGTO[a] [18] | Experiment[a] [17] |
|---|---|---|---|---|---|
| $1a_1$ | −20.555 000 1 | −20.554 265 1 | −20.564 731 | | −19.8 |
| $2a_1$ | −1.345 392 8 | −1.345 760 29 | −1.352 526 | | −1.18 |
| $1b_2$ | −0.709 262 | −0.711 834 43 | −0.718 069 | | −0.680 2 |
| $3a_1$ | −0.577 699 39 | −0.576 596 91 | −0.585 405 | | −0.541 7 |
| $1b_1$ | −0.504 568 24 | −0.504 200 74 | −0.509 114 | | −0.463 8 |
| Total energy | − 76.072 849 | −76.072 746 | −76.065 304 | −76.067 3 | |

[a] $H_2O$.

matrices, the angularly resolved photoionization cross section can be expressed as

$$\sigma_{fi}(E) = \frac{4}{3}\pi^2 \alpha a_0^2 \omega \sum_{ql_f m_f} |d_{ql_f m_f i}(E)|^2. \quad (8)$$

When averaged over molecular orientation and spin, the photoionization cross section will become

$$\left(\frac{d\sigma}{d\Omega}\right)_{AV} = \frac{\sigma}{4\pi}[1 + \beta P_2(\cos\theta)] \quad (9)$$

where $\beta$ is the asymmetry parameter and $P_2$ is the Legendre polynomial. Details of the R-matrix theory of photoionization are discussed in [13–15].

### 2.1. Target model

The photoionization cross section for $X_2O$ (where X is H or D throughout) in co-planar geometry was calculated based on the UK R-matrix method described in the previous section. The present study uses self-consistent field (SCF) molecular orbitals for the ground state in the configuration interaction (CI) calculation to deal with photoionization of the water molecule. Special attention was paid to the selection of basis set, the R-matrix radius ($r$) and the number of ionic states for the convergence of wave functions in the inner region. A suitable combination of these factors give convergence and produce the best results. Model calculations were performed varying ionic states to tackle the correlation problem and the final calculations were executed considering ionic states below $^2B_2$ of water. The target charge density was confined inside the R-matrix sphere of radius $r = 10a_0$ using the cc-pVTZ basis set. The configuration state functions for the molecular ion were generated employing four full valence complete active spaces (CASs) in the CI formalism. The number of configuration state functions generated to represent the ground state of the neutral and ionized targets were 508 and 640, respectively. Partial waves up to g ($l \leqslant 4$) are considered to represent the continuum orbitals since many excited states representing electronic transition show Rydberg character. These orbitals were used to construct the outer region problem. The orbital energies of neutral and ionized $X_2O$ are tabulated in tables 1 and 2, respectively. The R-matrix codes were implemented through Quantemol-N [16].

### 2.2. Target states

The $H_2O$ molecule has $C_{2v}$ symmetry when in equilibrium geometry. The bond lengths and angles are 1.809 $a_0$ and 104.478°, respectively, whereas for $D_2O$ the bond lengths and angles are 1.806 $a_0$ and 105.200°, respectively. It has a bent structure at equilibrium due to the presence of two lone pair electrons. The ground state for both the targets is doubly occupied and is represented as $1(a_1)^2$, $2(a_1)^2$, $1(b_2)^2$, $3(a_1)^2$, $1(b_1)^2$ . The outermost orbital contains lone pair electrons and the inner $3a_1$ and $1b_2$ orbitals contribute to bonding. The lowest energy transitions, $1b_1$ ($1^1B_1$) to $4a_1$ and $3a_1$ ($2^1A_1$) to $4a_1$ give rise two low-lying excited states at 7.61 and 9.36 eV, respectively [19]. The ground-state configuration of $X_2O^+$ is $1(a_1)^2$, $2(a_1)^2$, $1(b_2)^2$, $1(b_1)^2$, $3(a_1)^1$. The highest occupied orbital is singly occupied, hence electronic transition into this state gives rise to many excited states. The electronic transitions into excited states exhibit several sharp bands in the photoionization curve. These states are of great importance when studying the photoionization cross section. The calculations were carried out by CI (HF) approximation in the R-matrix method. The orbitals are represented as a sum of frozen and active orbitals as $(1a_1)^2$ and $(2a_1, 3a_1, 4a_1, 5a_1, 1b_1, 1b_2, 2b_2, 3b_2)^8$, respectively. For the $X_2O^+$ ion the frozen electron will remain the same and the other seven electrons are shared among eight active orbitals. The active orbitals are used to represent the electron–electron correlation in the target.

**Table 2.** SCF total and orbital energies of $X_2O^+$ (in au).

| Orbital | Present $H_2O^+$ | Present $D_2O^+$ |
|---|---|---|
| $1a_1$ | −21.091 540 2 | −21.091 540 2 |
| $2a_1$ | −1.809 536 8 | −1.810 271 8 |
| $1b_2$ | −1.187 370 7 | −1.189 943 2 |
| $3a_1$ | −0.995 906 7 | −0.996 274 21 |
| $1b_1$ | −0.600 851 47 | −0.600 483 97 |
| Total energy | −75.583 506 | −75.584 656 |

## 3. Results and discussion

The orbital energies of the ground-state configuration for the neutral and ionized target are shown in tables 1 and 2, respectively, together with previously reported data. The total photoionization curve is represented with respect to the wavelength scale and partial cross sections are studied in the energy scale for the purposes of comparison.

The present CI model with the cc-pVTZ basis gives good agreement with the reported results. The isotopic partner $D_2O$

**Table 3.** Vertical IP of different target state (in eV).

| State | $H_2O$ | $D_2O$ | Reference [21][a] | Reference [22][b] | FC SO [11] | TD-DFT [10] |
|---|---|---|---|---|---|---|
| $^2B_1$ | 12.541 | 12.640 | 12.61 | 12.62 | | 12.61 |
| $^2A_1$ | 14.651 | 14.540 | 14.73 | 14.74 | 12.18 | 14.73 |
| $^2B_2$ | 19.340 | 19.424 | 18.55 | 18.51 | | 18.55 |
| $^2B_1$ | 27.319 | 27.596 | | | | |
| $^2A_1$ | 27.374 | 27.910 | | | | |
| $^2B_1$ | 29.066 | 29.459 | | | | |
| $^2A_2$ | 29.239 | 29.516 | | | | |
| $^2B_2$ | 29.640 | 30.138 | | | | |
| $^2A_2$ | 30.785 | 31.150 | | | | |
| $^2A_2$ | 31.506 | 31.769 | | | | |
| $^2A_1$ | 32.113 | 32.385 | 32.20 | 32.20 | 31.57 | 32.20 |

[a] Photoelectron spectroscopy.
[b] Photoelectron spectroscopy.

shows only a 1% change from the normal species, $H_2O$. The vertical ionization potential (IP) of present target for all possible $X_2O^+$ ion states up to $^2A_1((2a_1)^{-1})$ are shown with the available experimental results in table 3. The present CI calculation agrees reasonably well with the reported experimental data. The calculated IP values for the first $X_2O^+$ ionic state reinforce Mulliken's prediction of the removal of a non-bonding electron from the oxygen atom [20].

The present cross sections for $X_2O$ show the presence of many bound states, which are true features of photoionization. However, these features are too sharp in the present calculation due to the approximation of fixed geometry and hence neglect of vibrational motions of the target.

### *3.1. Photoionization cross section*

We have calculated the photoionization cross section for $H_2O$ using the CI model. Figure 1 presents the photoionization cross section of $H_2O$ in the ultraviolet region. Our CI calculation shows good agreement with the experimental results. Above 87 nm the experimental data show oscillatory behavior in the cross section curve. Two prominent autoionization lines are observed in the experimental data of Hadad *et al* [6], which lie on features of the present result. The present multichannel cross section also has numerous sharp peaks, supporting the earlier work of Katayama *et al* and Al-Joboury *et al* [3, 23]. They observed the presence of more or less regularly spaced resonance peaks, which merge to a continuum around 86 nm. These are due to autoionization from Rydberg levels below the threshold of the $^2A_1$ state of the $H_2O^+$ ion. Due to the very small change in the Franck–Condon factors for the electronic transition, not all these features are visible in experimental studies [3]. The experiments in [23] show another group of lines due to an autoionizing Rydberg level that starts initially at around 78 nm and merges to a continuum around 69 nm (18 eV), which is the threshold value for the second ionic state ($^2A_1$) of $H_2O^+$. The present study obtained a threshold value for this state at 19.34 eV, showing excellent agreement with the experimental data of Brundle and Potts [21, 22] . Hence, the second series corresponds to autoionization converging to 64.5 nm

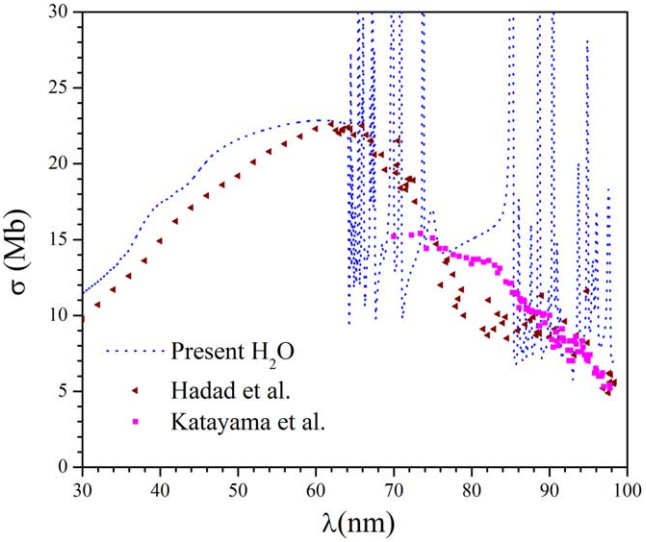


**Figure 1.** Photoionization cross section of $H_2O$.

(19.22 eV) for the present ionization curve. Some earlier work report the IP of the $^2A_1$ state as 16.2 eV and the enhancement near 16.2 eV as due to direct ionization. Later it was proved to be due to autoionizing transitions, as observed in the present curve [24].

The R-matrix calculation for the total photoionization cross section of $D_2O$ is reported in figure 2. The present calculation shows good agreement with the only reported experimental result of Katayama *et al* [3]. The isotope of $H_2O$ also supports many resonances like structures similar to $H_2O$ due to the same Rydberg transitions but with small shift due to the isotopic effect. The photoionization threshold obtained by the present calculation is 983 nm or 12.6 eV, which is very close to the convergence limit (12.62 eV) of the mean value of C and D Rydberg series [25]. For $D_2O$ the observed shift in IP is 0.02 eV.

The first ionization potential is a vertical transition to the continuum of one of the lone pair (basically a non-bonding electron of O atom) of $H_2O$ [26]. The experimental result shows high yield and a sharp break for both isomers. The present result also supports this feature. Two energy bands

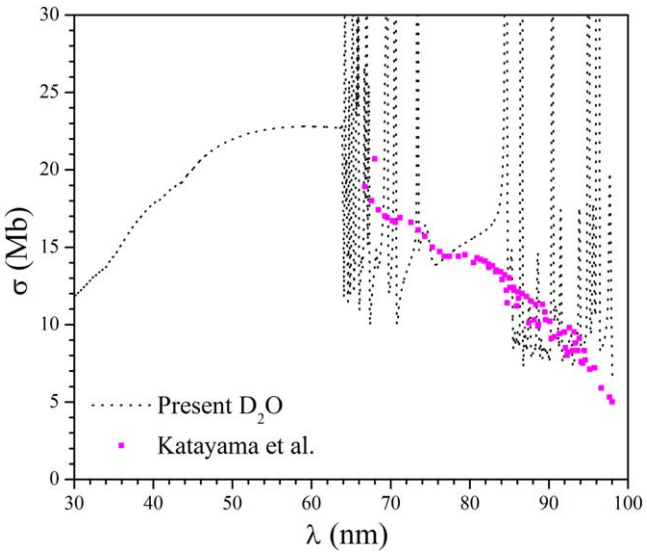


**Figure 2.** Photoionization cross section of $D_2O$ for 30–100 nm.

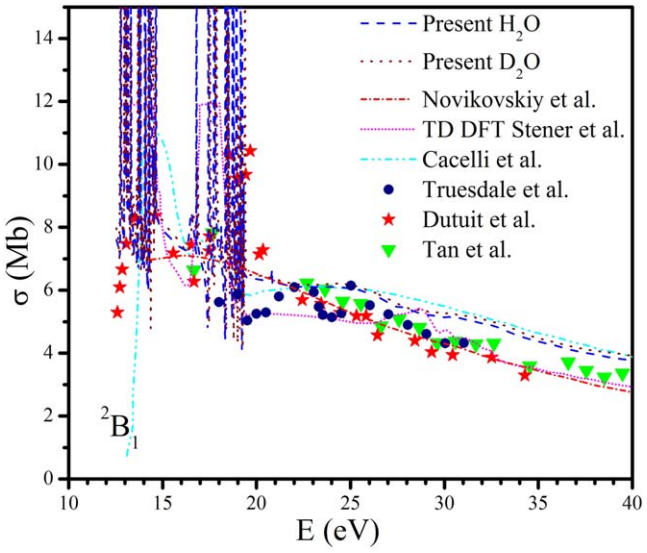


**Figure 3.** Partial photoionization cross section of the $1b_1$ orbital of $H_2O$ and $D_2O$.

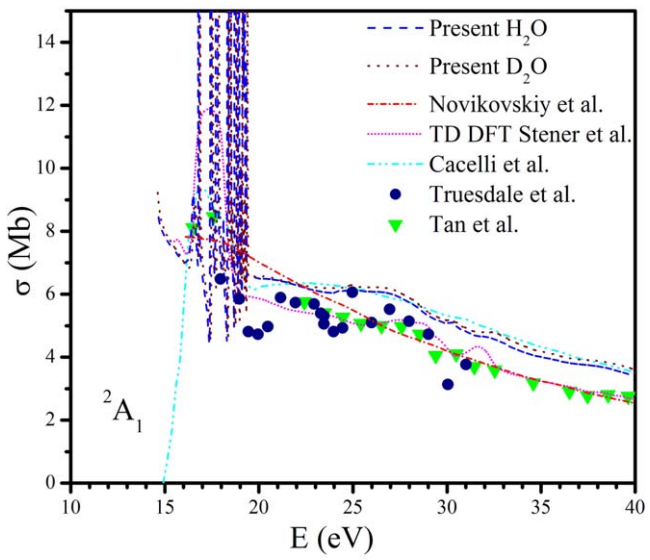


**Figure 4.** Partial photoionization cross section of the $3a_1$ orbital of $H_2O$ and $D_2O$.

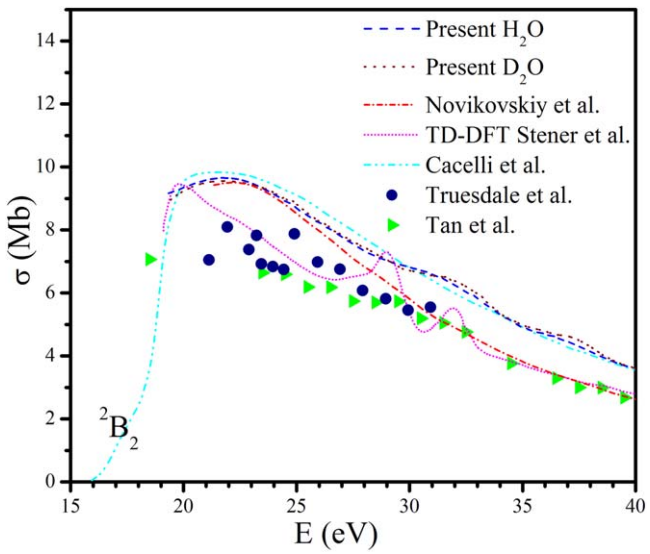


**Figure 5.** Partial photoionization cross section of the $1b_2$ orbital of $H_2O$ and $D_2O$.

were identified above the IP: a first series centered at 14 eV and a second at 18. These are the quasi bound states at the continuum. The oscillations appearing in the present ionization curve support Watanabe's [27] prediction of the presence of pre-ionized diffuse bands at 85–95 nm. The transitions between different states are given below:

$$1b_1 \rightarrow nsa_1, npa_1, nda_1; npb_1, ndb_1$$
$$3a_1 \rightarrow nsa_1, npa_1, nda_1$$
$$1b_2 \rightarrow nsa_1, npa_1, nda_1; npb_2, ndb_2. \quad (10)$$

The total cross section data are elucidated by reporting partial photoionization cross sections separately in figures. The contribution of different partial channels towards total photoionization is clearly seen from these figures. The reported curve for the present calculation shows many sharp lines for the electronic transitions given in equation (10).

## 4. Partial cross section of a valence-shell orbital

In the one-electron model the ground state of water is represented as $(1a_1)^2(2a_1)^2(1b_2)^2(3a_1)^2(1b_1)^2$. Among these, orbital $1a_1$ forms the innermost orbital, $2a_1$ is the inner valence orbital and the remaining three represent the outer valence orbital. The partial photoionization cross section of the three outer valence orbitals of $H_2O$ and its isotopic part is reported in figures.

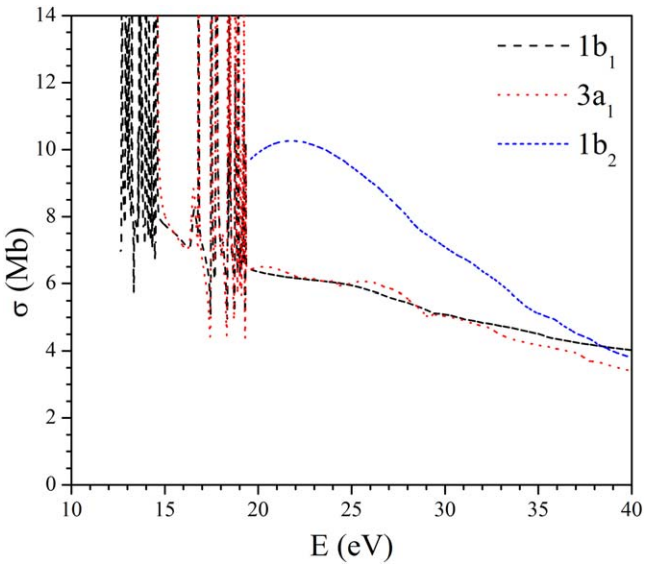


**Figure 6.** Comparison of partial photoionization cross section for three valence orbitals of $H_2O$.

### 4.1. State $1b_1$ (IP = 12.6)

Figure 3 shows the partial photoionization cross section for production of the $^2B_1((1b_1)^{-1})$ state of $H_2O^+$ and $D_2O^+$ from threshold up to 40 eV in step sizes of 0.02 eV. The present calculation produces many bound states and agrees reasonably well with experiments. However, it overestimates the experimental result of Dutuit *et al* [5]. This is partly attributed to a channel coupling effect which is not considered adequately in the present method. The result of Tan *et al* [8] shows better consistency with the present result. Truesdale *et al* [7] reported the cross section with oscillations and an autoionization peak for this state, but above the ionization threshold of the $3a_1$ electron. This can be attributed to the high ionization threshold calculated in their study. The present data show more closely spaced sharp resonance-like structures than the experiment below the third IP state, $(1b_2)^{-1}$. The experimentalists use a relatively broad energy bandpass (1.4 eV) which smooths out most of the Rydberg transition and autoionization structures that appear below the $(1b_2)^{-1}$ state. However, the experimental result of Dutuit *et al* [5] reports structures below 20 eV, which coincides with the present curve. The theoretical result of Cacelli *et al* [9], who used a K-matrix-based random phase approximation, agrees well with the present R-matrix result, except for Rydberg transitions near the threshold of the $^2B_1$ and $^2A_1$ states. The result of Cacelli *et al* [9] shows resonance in the cross section near the threshold of the $^2B_1$ state due to autoionization. Their result shows the presence of a weak resonance peak near 17 eV, which is also of the autoionization type. However, a change in peak position is observed due to change in the threshold value of two results. The TD-DFT result of Stener *et al* [10] also produced two autoionization peaks near the threshold of states $^2B_1$ and $^2A_1$. The recent result of Novikovskiy *et al* [11] by the SC method decreases monotonically, and autoionizing Rydberg features are absent in their study due to the neglect of many-electron correlations and various autoionizing resonant states. The present study resolved both autoionization and Rydberg transitions in the photoionization curve of the $^2B_1$ state. The sharp lines representing Rydberg transition into a bound state, which appear after absorption of an incident photon of a particular energy, are true features of a photoionization cross section. Earlier Delaney *et al* [28] also predicted the presence of a resonance-like structure for the $^2B_1$ state below 20 eV. The Rydberg transitions appearing in the cross section curve are consistent with the oxygen atom. This can be explained considering the orbitals of the $H_2O$ molecule. The $1b_1$ orbital is occupied by a lone pair electron of O ($P_x$). Hence, the photoionization curve for this state is quite analogous to atomic oxygen as reported in previous works [29, 30]. The quantitative change in photoionization cross section due to the heavier isotope is only 1%.

### 4.2. State $3a_1$ (IP = 14.6)

The photoionization cross section for state $3a_1$ is shown in figure 4. The oscillation for state $^2A_1((3a_1)^{-1})$ starts above 14.6 eV, the orbital IP for state $(3a_1)^{-1}$ . This state has significant involvement with H atoms. Hence, sp hybridization is present for this state. Here we observed a mixed effect of O and H atoms in Rydberg transitions due to $\sigma$ bonding.

The first bound state is observed at 16.5 eV, which is 1 eV higher than the IP of the $H_2$ molecule. Present data points appear to have the same shape but overestimate the experimental result of Tan *et al* [8]. The nature of Truesdale *et al*'s [7] data is same for this state as for $^2B_1$. The reason for this is the same as that discussed above. The results of Cacelli *et al* [9] show good agreement with the $^2B_1$ state. The TD-DFT result [10] reported a smaller value for the cross section. The TD-DFT result produced an autoionization peak centred at 17.5 eV, which is 1 eV higher than the present result. The present study resolves autoionizing Rydberg series below the $^2B_2$ state. The nature of the cross section in [11] is same as that of the $^2B_1$ state.

### 4.3. State $1b_2$ (IP = 19.6)

Figure 5 represents the photoionization cross section for the $1b_2$ orbital. The cross section for this state is enhanced due to a bonding effect. The $1b_2$ orbital takes part in bonding, where the $\sigma^*$ orbital of the $H_2$ molecule hybridizes with O($2P_y$). *Ab initio* study reveals that this state is a strongly bent state [24]. The resonance-like behavior is actually due to a bonding effect. To confirm this we used the Breit–Wigner formula and observed no change in sign in the eigen-phase curve. Also, the energy of this state is above the dissociation limit of $H_2O$. Hence, enhancement of the cross section is observed. The present result for this state does not agree well with the experimental [7, 8] cross section quantitatively, but their nature remains the same. The result of Cacelli *et al* [9] is slightly higher than the present calculation below 30 eV. This can be attributed to the neglect of adequate correlation effects. The inconsistency of the present result with those of Stener *et al* [10] is maximum for this state. This may be rectified by using a large number of target ionic states. However, this

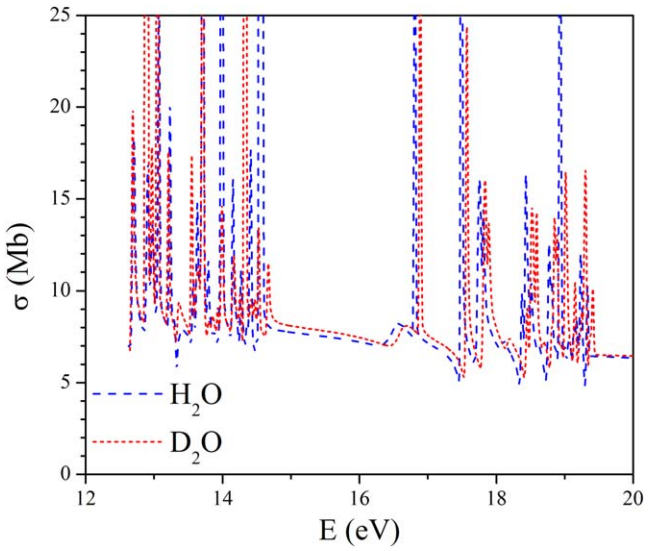


**Figure 7.** Comparison of Rydberg transitions for $H_2O$ and $D_2O$.

causes higher correlations, which reduces the value of the cross section, greatly increasing the ionization threshold of each orbital and diminishing the bonding effect. The result of Novikovskiy *et al* [11] agrees very well with the present calculation up to 25 eV; above this their data decrease monotonically, whereas the present result remains consistent with Cacelli *et al* [9].

A comparison of the photoionization cross section for the valence orbitals of $H_2O$ is presented in figure 6. The inconsistency of OH bonding is clearly visible in this figure. Figure 7 shows a comparison with $D_2O$ of the total photoionization cross section of autoionizing Rydberg states. A shift in different autoionizing Rydberg series is obtained. This is due to the change in vertical IP values of different states of $H_2O$ and $D_2O$. This is clearly visible from the partial photoionization curve of the $1b_1$ valence shell of water (figure 3). Thus, a shift in the total photoionization cross section is observed. A few extra features are also identified for $D_2O$; these are due to the presence of extra Rydberg states.

## 5. Conclusion

Several theoretical and experimental studies on the photoprocesses of water have been reported to date. However, these studies have not been able to successfully resolve the near-threshold features—hence they fail to give a complete description of the photon interaction processes. The present R-matrix study gives a comprehensive theoretical representation of photoionization cross sections for $H_2O$ and $D_2O$, which resolve the near-threshold features successfully under the fixed nuclei approximation. Use of a large SCF function to construct ground-state wave function in the CI approximation gives a satisfactory result for the vertical IP values for the outer and inner valence orbitals of water. The values of state energy reported agree well with the experimental and theoretical data.

The photon-induced cross section using the cc-pVTZ basis set gives good agreement with the reported experimental and other theoretical results for $H_2O^+$ ionic states. The calculated partial photoionization cross section for the outer valence shells $(1b_1^{-1})X^2B_1$ and $(3a_1^{-1})^2A_1$ are found to agree well with the available experimental and theoretical results. For the $(1b_2^{-1})^2B_2$ state the present calculation shows a higher cross section than the previous experimental result. Several lines are observed in the photoionization curve for the final calculation. They arise due to transition from the inner valence shell, thus forming bound states. This gives rise to several features in the ionization continuum. Hence, a number of virtual orbitals are observed corresponding to these bound states. These states have an important role in the autoionization process.

For the $^2B_1$ state, the present calculation shows good agreement with Katayama *et al* [3]. The data of Dutuit *et al* [5] also show some features which are resolved in the present calculation. Among the three valence states of $H_2O$ better agreement was found for the $^2B_1$ and $^2A_1$ states. For the $^2B_2$ state, the present calculation reports a larger cross section than for the other two states. The experiments also suggest a larger cross section for this state, but the present data points are much higher than previous experimental data. This is consistent with the discrepancy of the O–H bonding orbital of $H_2O$. However, the effects of correlation need to be accounted for to resolve the bonding effect accurately. Inadequate description of correlation causes a high cross section value, whereas over-correlation diminishes it by increasing the ionization threshold of each orbital. This problem is minimized adequately in the present R-matrix calculation using a better description of electron correlation in the CI configuration.

The isotopic effect is also studied in the present calculation. The present study shows an isotopic shift in the cross section curve. The change in cross section due to the heavier isotope is quite marginal, with some extra features in Rydberg transitions. This is due to a small change in bond length and bond angle. The calculated isotope-specific photoionization cross sections will help in accurately determining rate coefficients and attenuation coefficients for $H_2O$ in various chemical environments. In general, the present calculations with a step size of 0.02 eV produce reliable cross sections for the interaction of photons with water and its isomeric counterpart. Thus, the present results for $H_2O$ and $D_2O$ will be valuable inputs in astrochemistry modeling and ion–molecule chemistry, being the first for valence-shell photoionization of $D_2O$.

## Acknowledgments

The authors wish to acknowledge assistance from the Quantemol-N support team. The authors also acknowledge financial support from ISRO, project number DS-2B-13012(2)/2/2017.

## ORCID iDs

Bobby Antony https://orcid.org/0000-0003-2073-9681

## References


[1] Gallagher J W, Brion C E, Samson J A R and Langhoff P W 1988 *J. Phys. Chem. Ref. Data* **17** 9–153
[2] Croteau P, Randazzo J B, Kostko O, Ahmed M, Liang M C, Yung Y L and Boering K A 2011 *Astrophys. J.* **728** L32
[3] Katayama D H, Huffman R E and O'Bryan C L 1973 *J. Chem. Phys.* **59** 4309–19
[4] Martin U S, Klaus L and JüRgen T 1993 *Ber. Bunsengesell. Phys. Chem.* **97** 953–60
[5] Brion C and Carnovale F 1985 *Chem. Phys.* **100** 291–6
[6] Haddad G N and Samson J A R 1986 *J. Chem. Phys.* **84** 6623–6
[7] Truesdale C M, Southworth S, Kobrin P H, Lindle D W, Thornton G and Shirley D A 1982 *J. Chem. Phys.* **76** 860–5
[8] Tan K, Brion C, der Leeuw P V and van der Wiel M 1978 *Chem. Phys.* **29** 299–309
[9] Cacelli I, Carravetta V and Moccia R 1992 *J. Chem. Phys.* **97** 320–6
[10] Stener M, Fronzoni G, Toffoli D and Decleva P 2002 *Chem. Phys.* **282** 337–51
[11] Novikovskiy N, Sukhorukov V and Artemyev A E A 2019 *Eur. Phys. J.* D **73** 1–8
[12] Morgan L A, Tennyson J and Gillan C J 1998 *Comput. Phys. Commun.* **114** 120–8
[13] Harvey A G, Brambila D S, Morales F and Smirnova O 2014 *J. Phys. B: At. Mol. Opt. Phys.* **47** 215005
[14] Burke P G and Taylor K T 1975 *J. Phys. B: At. Mol. Phys.* **8** 2620
[15] Tennyson J 2010 *Phys. Rep.* **491** 29–76
[16] Tennyson J, Brown D B, Munro J J, Rozum I, Varambhia H N and Vinci N 2007 *J. Phys.: Conf. Ser.* **86** 012001
[17] Müller-Plathe F and Diercksen G H F 1989 *Phys. Rev.* A **40** 696–711
[18] Bawagan A, Brion C, Davidson E and Feller D 1987 *Chem. Phys.* **113** 19–42
[19] Elles C G, Rivera C A, Zhang Y, Pieniazek P A and Bradforth S E 2009 *J. Chem. Phys.* **130** 084501
[20] Mulliken R S 1955 *J. Chem. Phys.* **23** 1833–40
[21] BrundJe C and Turner D 1968 *Proc. R. Soc.* A **307** 27–36
[22] Potts A and Price W 1972 *Proc. R. Soc.* A **326** 181–97
[23] Al-Joboury M I and Turner D W 1964 *J. Chem. Soc.* 4434–41
[24] Leclerc J, Horsley J and Lorquet J 1974 *Chem. Phys.* **4** 337–52
[25] Price W C 1936 *J. Chem. Phys.* **4** 147–53
[26] Mulliken R S 1935 *J. Chem. Phys.* **3** 506–14
[27] Watanabe K and Jursa A S 1964 *J. Chem. Phys.* **41** 1650–3
[28] Delaney J J, Saunders V R and Hillier I H 1981 *J. Phys. B: At. Mol. Phys.* **14** 819
[29] Bell K L, Burke P G, Hibbert A and Kingston A E 1989 *J. Phys. B: At. Mol. Opt. Phys.* **22** 3197–204
[30] Berkowitz J 1997 *J. Phys. B: At. Mol. Opt. Phys.* **30** 583–92